RZ 3949 (#ZUR1904-029) 04/10/2019
Physical Sciences 4 pages

# Research Report

## Microcavity Lasers on Silicon by Template-Assisted Selective Epitaxy of Microsubstrates

Benedikt F. Mayer, Stephan Wirths, Svenja Mauthe, Philipp Staudinge, Marilyne Sousa, Joel Winiger, Heinz Schmid, Kirsten E. Moselund

IBM Research – Zurich
8803 Rüschlikon
Switzerland

© 2019 IEEE. Personal use of this material is permitted. Permission from IEEE must be obtained for all other uses, in any current or future media, including reprinting/republishing this material for advertising or promotional purposes, creating new collective works, for resale or redistribution to servers or lists, or reuse of any copyrighted component of this work in other works.

This is the accepted version of the article published by IEEE (early access): Benedikt F. Mayer, Stephan Wirths, Svenja Mauthe, Philipp Staudinge, Marilyne Sousa, Joel Winiger, Heinz Schmid, Kirsten E. Moselund, "Microcavity Lasers on Silicon by Template-Assisted Selective Epitaxy of Microsubstrates," in IEEE Photonics Technology Letters.
10.1109/LPT.2019.2916459

LIMITED DISTRIBUTION NOTICE

This report has been submitted for publication outside of IBM and will probably be copyrighted if accepted for publication. It has been issued as a Research Report for early dissemination of its contents. In view of the transfer of copyright to the outside publisher, its distribution outside of IBM prior to publication should be limited to peer communications and specific requests. After outside publication, requests should be filled only by reprints or legally obtained copies (e.g., payment of royalties). Some reports are available at http://domino.watson.ibm.com/library/Cyberdig.nsf/home.

**Research**
**Africa • Almaden • Austin • Australia • Brazil • China • Haifa • India • Ireland • Tokyo • Watson • Zurich**

This article has been accepted for publication in a future issue of this journal, but has not been fully edited. Content may change prior to final publication. Citation information: DOI 10.1109/LPT.2019.2916459, IEEE Photonics Technology Letters



# Microcavity Lasers on Silicon by Template-Assisted Selective Epitaxy of Microsubstrates

*Benedikt F. Mayer‡, Stephan Wirths‡, Svenja Mauthe, Philipp Staudinger, Marilyne Sousa, Joel Winiger, Heinz Schmid and Kirsten E. Moselund*

**Abstract— The vision of microchips that benefit from the high data rates of optical links has recently lead to novel concepts for the monolithic integration of active gain materials on silicon. In this work, we use template-assisted selective epitaxy (TASE) for the monolithic integration of GaAs microsubstrates on silicon which allow the subsequent integration of lattice-matched III-V laser cavities. We demonstrate room-temperature operation of optically pumped microdisk-lasers with hexagonal top-facets and diameters as low as 1.2µm. The devices exhibit uniform emission spectra, low lasing thresholds of Pth=13.6 ± 0.7 pJ/pulse and a high temperature stability ($T_0$=370K). Scanning electron microscope and photoluminescence analysis of larger devices with a flat top-facet reveal a rotation of the crystal orientation and further reduced lasing thresholds. Our results show that monolithic integration of III-V micro-substrates on silicon offer a versatile platform for on chip light sources with excellent optical properties.**

**Microlaser, Microsubstrate, Monolithic integration, Silicon photonics**

## I. Introduction

Transmitting data with the speed of light and at high data rates enabled by wavelength division multiplexing have rendered optical links indispensable for modern data traffic. Emerging technology markets such as the internet of things and implementation of artificial intelligence are expected to further increase the data traffic significantly. This will also augment the interest in bringing optical interconnect technology onto the chip itself. A key component missing to facilitate this is an economic integration of small form factor and low power light sources on the silicon chip. Therefore, solutions to bypass the limitations of the indirect nature of the silicon band structure by incorporating better suited materials are urgently needed. Significant progress has been achieved by integrating III-V gain material monolithically on silicon for photonic devices [1][2][3]. We have developed a technique referred to as Template-Assisted Selective Epitaxy (TASE) which allows for the local selective growth of various III-Vs within oxide templates[4][5]. Using this TASE method, we have demonstrated the integration of III-Vs on several Si crystal orientations [6] as well as co-planar integration of multiple III-Vs on silicon [7]. Recently, the excellent material quality achieved by the growth of III-V nanowires on silicon and consequent demonstrations of their lasing operation have also fueled the vision of monolithically integrated nanophotonic devices as future coherent light sources [8]. Optically pumped nanowire lasers have been shown to operate at lasing wavelengths below the silicon bandgap [9], provide ultrafast gain dynamics [10][11] and allow the integration of quantum heterostructures [12]. Alternatively, microring and microdisk laser geometries are desirable for small form-factor silicon photonics applications due to their high quality (Q)-factors and evanescent waveguide coupling. We recently reported on the fabrication of mushroom-shaped microdisk lasers on Si [13]. Here, this work is extended to the integration of GaAs microsubstrates, from which microring and microdisk geometries are fabricated using a second growth step. The devices demonstrate optically pumped room-temperature lasing operation on silicon. While the approach based on microsubstrates requires an additional epitaxy step, as compared to the previous approach [13], it offers the possibility for more complex vertical material compositions such as vertical doping profiles for electrical actuation and incorporation of quantum wells (QWs). The latter was conceptually demonstrated based on an InP microsubstrate [14]. Furthermore, the approach presented in this manuscript allows to control the lateral shape of the microcavity and thus allows the fabrication of tailored lateral cavity designs. In contrast, the lateral cavity design of our previous approach [13] and of typical III-V nanowire laser devices [11][12] is determined by the (e.g. hexagonal) crystal structure of the gain material**.** Hence the two approaches are distinct and complementary with respect to future device integration, the direct growth in [13] only allows for the integration of QWs and/or doping profiles in the radial direction as the growth proceed from a central seed. Whereas the approach via the micro-substrate which we reveal here, allows for the integration of QWs in the vertical stack as for conventional laser stacks, with the added benefit that there is no need for etching of the III-V sidewalls, which are grown directly into the cavity defined by the second template.

Manuscript received February 3, 2019. The research leading to these results has received funding from the ERC Starting Grant project under Grant Agreement No. 678567 “PLASMIC” and European Union's Horizon 2020 research and innovation program under grant agreement No. 704045 “MODES”. Corresponding Author: kmo@zurich.ibm.com. The manuscript was written through contributions of all authors. ‡These authors contributed equally. The authors would also like to thank Dr. L. Czornomaz for fruitful discussions and M. Tschudy for his support. The authors are with IBM Research Zurich, Säumerstrasse 4, 8803 Rüschlikon, Switzerland.

Copyright (c) 2019 IEEE

1041-1135 (c) 2019 IEEE. Personal use is permitted, but republication/redistribution requires IEEE permission. See http://www.ieee.org/publications_standards/publications/rights/index.html for more information.

This article has been accepted for publication in a future issue of this journal, but has not been fully edited. Content may change prior to final publication. Citation information: DOI 10.1109/LPT.2019.2916459, IEEE Photonics Technology Letters


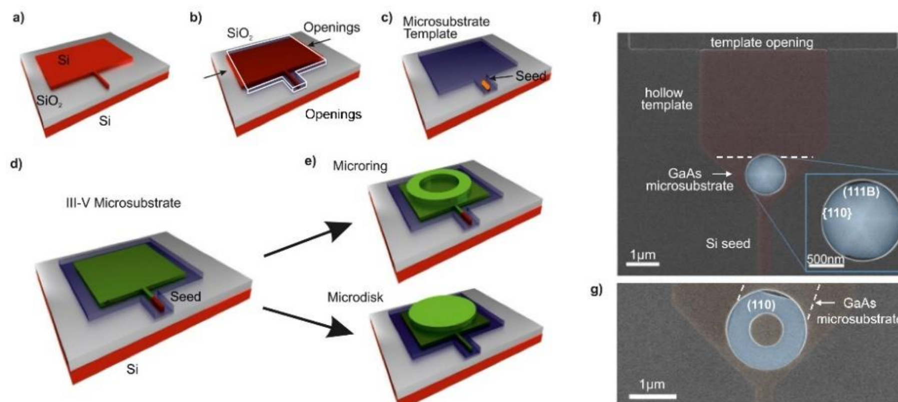


**Figure 1**. a)-e) Schematic illustration of the fabrication process of Microcavity lasers grown on microsubstrates on silicon using template assisted epitaxy. (f) Laser device (device T3) with expected crystal orientation (standard lasers). The scale bar is 1µm. (g) Laser device (device F2) with unexpected crystal growth orientation (flat-top lasers). Dashed lines indicate the extension of the microsubstrate. Both template designs are shown: the square shape (a-e) and the funnel shape (f,g).

## II. Device Fabrication

The laser structures are grown by Metal-Organic Chemical Vapor Deposition (MOCVD) on silicon on insulator (SOI) substrates as illustrated in Figure 1. First, the top silicon layer of an SOI wafer is thinned down to a thickness of 60 nm by a combination of oxidation and hydrofluoric acid (HF) etching of the thermal oxide, which is done to keep the nucleation area small. In the next step, the thin silicon film is structured by a combination of electron beam lithography and inductively coupled plasma dry etching using an HBr chemistry to define the extension of the microsubstrate. The size of the microsubstrate is adjusted to a couple of square µm to avoid excessively long growth times, which also might lead to parasitic growth. For the shape of the templates we chose squared shaped designs and funnel shaped structures as shown by the schematic illustrations and the SEM images in Fig. 1, respectively. As shown in Fig. 1 a), the microsubstrate (red) extends from a lithographically defined silicon nanowire which acts as growth seed for the III-V material. The purpose of the silicon NW is to limit the nucleation to a single point to avoid dislocation formation at the heterojunction. We started out with an SOI substrate which provides high dielectric isolation to the bottom Si substrate, has good thickness uniformity and a smooth top surface. We note that the fabrication can also be implemented based on a regular silicon wafer similar to Czornomaz et al. [5] or Wirths et al. [13]. In the next step (Fig. 1b), the structured silicon layer is covered by a 20 nm thin $SiO_2$ layer deposited by atomic layer deposition (ALD) followed by a plasma enhanced chemical vapor deposition (PECVD) of 200nm $SiO_2$. A second electron beam lithography and HF etching step are used to define openings to the silicon layer. The openings are used for the subsequent back-etching step using $XeF_2$ dry etching. The $XeF_2$ etch is timed to leave a small nucleation seed within the NW region, as shown in Figure 1c). Afterwards, immediately before growth the sample is cleaned in boiling Piranha etch (2:1 ratio $H_2SO_4$:$H_2O_2$) and a short BHF dip is done to remove native oxide at the seed. The sample is loaded in the MOCVD chamber and growth of the Si seed, as schematically depicted in Figure 1d). Subsequently, the GaAs microsubstrate (green) is grown according to [13] using trimethylgallium (TMGa) and tertiarybutylarsine (TBAs) at 600°C with a V-III ratio of 30. The structure extends from the silicon (red) to a ~2x2µm rectangular GaAs region inside the dielectric template. After completing the growth, another 300nm of PECVD oxide is deposited on the sample resulting in a total thickness of about 500nm. As shown by the example of the microring and the microdisk presented in Figure 1e), openings in the dielectric layer on top of the microsubstrate can now be structured using a combination of electron beam lithography and oxide etching. The ring and disk structures are transferred into the template oxide by reactive ion etching of the first ~450nm of the template structure, followed by HF wet etching of the residual template inside the ring to avoid exposure of the III-V surface to the impact of reactive ion etching. A second growth step is used to fill the micro-cavity template forming the desired device structure on top of the microsubstrate. A representative finished device is shown in Fig. 1f). Here the crystal facets evolved in accordance to the underlying (100) substrate and the specific growth conditions into a pyramidal structure with the resulting facets indexed in the figure. However, in a few devices, we also observe a single, planar top-facet, as illustrated in Fig. 1 g). Simulations show that the Q-factor improves for a flat top facet device. We therefore included this geometry in our analysis to serve as reference device as discussed later. Therefore, such a flat-top device is analyzed in detail as shown in Fig. 2.

The structural analysis by transmission electron microscopy (TEM) is shown in Fig. 2. It indicates that the microsubstrate close to the silicon seed is 10° tilted, and close to the cavity switches to a [-110] orientation. While the cause of this growth anomaly is not known, the resulting microsubstrate and microdisk, respectively is [-110] oriented. High resolution images in different areas show that the cavity is single crystalline with a (110) surface on top. Anti-phase boundary defects and threading dislocations were not observed, and potential defects at the homoepitaxial interface from the two growth steps were not detected. In the following, we compare devices with hexagonal top facets, and for the flat top devices we compare a ring and a disk laser. Figure 3) shows the optical response from the microdisk structure shown in Figure 1f), recorded at room-temperature (300K) and for increasing

1041-1135 (c) 2019 IEEE. Personal use is permitted, but republication/redistribution requires IEEE permission. See http://www.ieee.org/publications_standards/publications/rights/index.html for more information.

This article has been accepted for publication in a future issue of this journal, but has not been fully edited. Content may change prior to final publication. Citation information: DOI 10.1109/LPT.2019.2916459, IEEE Photonics Technology Letters


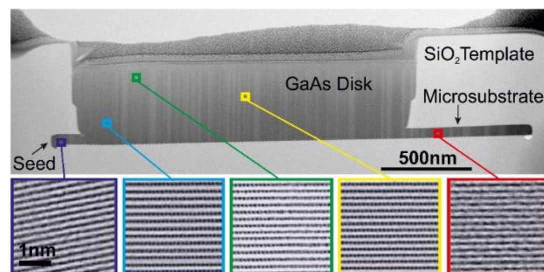


**Figure 2.** Structural analysis of a flat-top reference device. Low resolution BF-TEM image of the microsubstrate, the filled laser disk GaAs (top) and high-resolution STEM images (below). The vertical lines in the cavity on the overview image is a result of shadowing during the FIB process.

excitation powers. For excitation powers below 10pJ/pulse, we detect a ~50nm broad spontaneous emission peak around 875nm (1.42eV) which we attribute to the direct bandgap transition of GaAs (1.41eV) (Figure 3b, red curve).

## III. Optical properties of the microdisk lasers with hexagonal top facets

For excitation powers exceeding the lasing threshold of 10pJ/pulse, a sharp peak (black curve) is emerging from the spontaneous emission which at excitation powers of P=14.5 pJ/pulse (blue curve) is >70x stronger than the spontaneous emission.increasing excitation powers.(300K) and for increasing excitation powers. Under the strongest excitation (green curve, P=22.9 pJ/pulse), a dominant peak with a linewidth of 3nm is established. The strong linewidth narrowing accompanied by the sudden increase of the output intensity are both strong indications of the lasing operation of the devices. The room-temperature lasing of the devices is further supported by the characteristic S-shaped Light in-Light out (LL)-curve plotted on a log-log scale in Figure 3c). We next investigate the variation among the optical properties of five microdisk structures all with very similar diameters of 1.16±0.02µm and shape (T1, T2, T3, T4, T5), and two flat-top reference devices (F1 a disk, with a diameter of 1.9µm, and the ring cavity F2 with an inner diameter of 0.5µm and an outer diameter of 1.6µm) (Figure 4.a). The optical response under strongest excitation (P=22.9 pJ/pulse) is shown in Figure 4d) measured at room-temperature (red) and at 40K. As a consequence of the similarity of the laser cavities, the lasing peaks show a high overlap of the wavelength of the cavity mode and are centered around $\lambda_c$=862±5nm at room-temperature (red) and $\lambda_c$=799±5nm at 40K (blue). The corresponding wavelength shift of the lasing mode of $\Delta\lambda_T$=63nm correlates with the expected shift of the GaAs bandgap which, according to the Varshni's law, results in $\lambda_T$=54nm. Hence, we can conclude that the overlap of the spontaneous emission shifts enough with respect to the free spectral rage to accommodate lasing in a different mode at lower temperatures. The laser spectra (T1-T5) presented in Fig. 4b) exhibit a single lasing peak at room-temperature and single mode operation. At low temperature, most devices show a single lasing peak, while device T2 and T3 exhibit a second lasing peak around 845nm. We use this second lasing peak to determine the free spectral range of the presented lasers (T1-5) to $\lambda_T$=50nm. Figure 4c) and 4d) present the LL-curves for the devices (filled circles) for 40K and 300K,

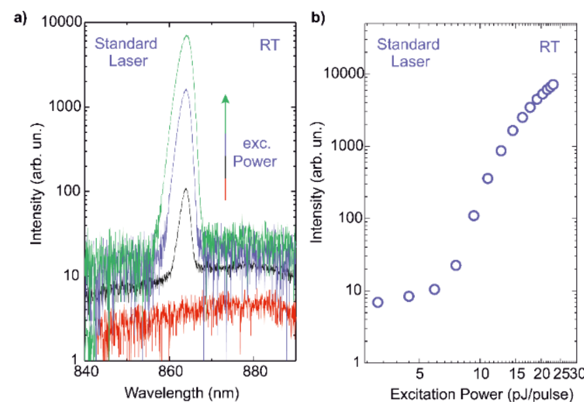


**Figure 3.** a) Room-temperture emission spectra of a microdisk laser (device T3), recorded at different excitation powers of 6pJ/pulse (red), 10pJ/pulse (black), 14.5pJ/pulse (blue) and 22.9pJ/pulse (green). b) Characteristic Light-in-Light-out curve of the microdisk laser shown in (a) plotted on a log-log scale.

respectively. The LL-curves are plotted on a lin-lin scale allowing a comparison of the lasing thresholds between measurements at 40K and room-temperature. All curves exhibit a clear kink indicating the onset of lasing from which we extract an average threshold value of $P_{th}$=13.6 ± 0.7 pJ/pulse at room-temperature and $P_{th}$=7.0 ± 1.4 pJ/pulse obtained at 40K. As a result, the excitation power required to reach the lasing threshold at room-temperature is only a factor of two higher than at 40K. From this, we obtain a remarkably high value of $T_0$=370K which is even comparable to the temperature stability of quantum dot lasers [15]. Interestingly, comparable values have been reported for quantum-dot microdisk lasers [1] and mushroom lasers [13] with comparable sizes. The large spectral range provided by small cavity lasers can easily lead to large energy offsets between the peak gain and the lasing mode. While for a specific temperature the cavity mode is well aligned to the gain spectrum and provides low lasing thresholds, other temperatures may require strong band filling and high pump powers before population inversion at the spectral position of the cavity mode can be reached. Assuming a more favorable spectral position of the lasing mode with respect to the gain spectrum at room-temperature compared to low-temperature operation could explain the high temperature stability found for small laser cavities with a large free-spectral range.

## IV. Comparison of the microdisk lasers with larger flat-top devices

Figure 4b) also shows the emission spectra of the two flat-top lasers in the range between 780nm and 1000nm obtained from a wavelength scan during strongest excitation of the devices (P=22.9 pJ/pulse). Remarkably, both flat-top devices exhibit very similar spectral emission signatures as the room-temperature lasing peak is accompanied by a small side-peak and the spectra are red-shifted compared to the spectra of the standard lasers. The characteristic input output curves for the microdisk and the microring laser measured at 40K and at room temperature are presented in Fig. 3c) and Fig. 3d), respectively. Again, the LL-curves of the microdisk and the microring exhibit a distinct "kink" at a lasing threshold of $P_{th}$=7.9pJ/pulse for the microdisk and Pth=8.8pJ /pulse for the microring laser at room temperature, both being significantly lower than the

1041-1135 (c) 2019 IEEE. Personal use is permitted, but republication/redistribution requires IEEE permission. See http://www.ieee.org/publications_standards/publications/rights/index.html for more information.

This article has been accepted for publication in a future issue of this journal, but has not been fully edited. Content may change prior to final publication. Citation information: DOI 10.1109/LPT.2019.2916459, IEEE Photonics Technology Letters



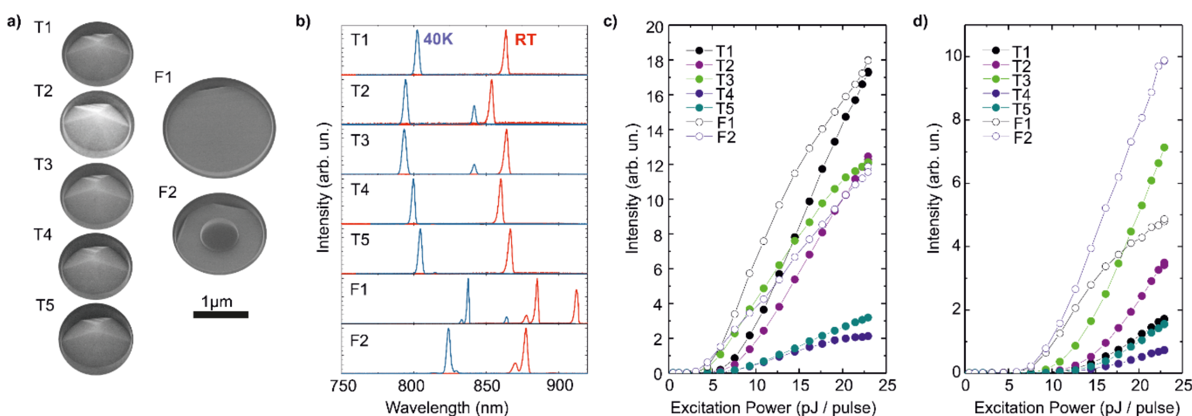


**Figure 4.** a) Scanning electron microscope image of the hex-top lasers (T1, T2, T3, T4, T5) and the flat-top lasers (F1, F2). b) Room-temperature emission spectra (red) and emission spectra recorded room temperature (RT, red) and at 10K (blue) of the different devices. c) LL-curves of the different devices recorded at 40K and plotted on a lin-lin scale. d) LL-curves of the different devices recorded at room-temperature and plotted on a lin-lin scale.

average threshold value of $P_{th}$=13.6 ± 0.7 pJ/pulse found for the standard lasers. The same trend is observed for the low temperature measurements where a lasing threshold of $P_{th}$= 4.4pJ/pulse is measured for the microdisk, 3.4pJ/pulse is measured for the microring and an average threshold of $P_{th}$=7.0 ± 1.4 pJ/pulse was found for the standard lasers. The results correspond again to high temperature stability factors of $T_0$=440K in case of the microdisk and $T_0$=270K in case of the microring. In order to compare the cavity Q-factors of the different devices we use finite difference time domain simulations (Lumerical software) to calculate the optical power in the cavities as a function of time. Fitting the decay with an exponential function in a simulation time interval between 1ps and 8ps, we calculate the corresponding cavity Q factor of the devices. Comparing the Q-factor of a hex-top and a flat-top microdisc, both with a diameter of d=1.16µm, we obtain a Q-factor of Q=975 for the hex-top device and a Q-factor of Q=1211 for the flat-top device, respectively. Simulating the optical power decay in a larger device with d=1.9µm and a flat top as device F1, we find a significantly enhanced cavity confinement with Q>7000. Therefore, we attribute the significant reduction of the lasing threshold of the two flat-top devices to the enhanced cavity confinement and cavity Q-factor provided by the larger diameter and flat top facet of these lasers.

## V. Conclusion

In summary, we demonstrated microdisk and microring laser monolithically integrated on silicon via microsubstrates that exhibit optically pumped room-temperature lasing. The advantage of this approach is that the geometry of the laser cavity may be defined freely by e-beam or optical lithography, so that no etching of the III-V gain medium is required. Secondly the use of purely lithographic techniques to define the position of the microcavities allows for the dense integration with silicon passives or electronic devices. The five investigated lasers have similar cavity dimensions, show remarkably reproducible lasing wavelength and exhibit single mode lasing operation. The low room-temperature lasing threshold of $P_{th}$=13.6 ± 0.7 pJ/pulse reduces to $P_{th}$=7.0 ± 1.4 pJ/pulse at 40K, which corresponds to a high temperature stability ($T_0$=370K) of the devices. A further reduction of the room-temperature lasing threshold down to $P_{th}$=7.9pJ/pulse was observed for the flat-top reference devices, as a result of the improved Q-factor. The very similar characteristics of the flat-top ring- and disk lasers however, indicate that the optical mode is primarily located along the perimeter of the device, which is also expected from a whispering gallery mode. Overall, the presented approach offers a promising technique for the monolithic integration of micro-lasers on silicon.

## References


1. Shi, B. *et al.* "1.55 um room-temperature lasing from subwavelength quantum-dot microdisks directly grown on (001) Si". *Applied Physics Letters* **2017**, *110*, 121109.
2. Wan, Y. *et al.* "Sub-wavelength InAs quantum dot micro-disk lasers epitaxially grown on exact Si (001) substrates". *Applied Physics Letters* **2016**, *108*, 221101.
3. Wang, Z. *et al.* "Room Temperature InP DFB Laser Array Directly Grown on (001) Silicon". *Nature Photonics* **2015**, *9*, 837.
4. Schmid, H. *et al.* **"**Template-assisted selective epitaxy of III-V nanoscale devices for co-planar heterogeneous integration with Si". *Applied Physics Letters* **2015**, *106*, 233101.
5. Czornomaz, L. *et al.* "Confined Epitaxial Lateral Overgrowth (CELO): A novel concept for scalable integration of CMOS-compatible InGaAs-on-insulator MOSFETs on large-area Si substrates". *VLSI Technology* **2015**, *2015 Symposium*, T172 - T173.
6. Borg, M. *et al.* "Vertical III-V Nanowire Device Integration on Si(100)". *Nano Letters* **2014**, *14*, 1914-1920.
7. Borg, M., *et al.* "High-Mobility in GaSb Nanostructures Cointegrated with InAs on Si". *ACS Nano* **2017**, *11*, 2554-2560.
8. Stettner, T. *et al.* "Direct Coupling of Coherent Emission from Site-Selectively Grown III–V Nanowire Lasers into Proximal Silicon Waveguides". *ACS Photonics* **2017**, *4 (10)*, 2537–2543.
9. Schuster, F. *et al.* "Site-Controlled Growth of Monolithic InGaAs/InP Quantum Well Nanopillar Lasers on Silicon". *Nano Letters* **2017**, *17 (4)*, 2697–2702.
10. Röder, R. *et al.* "Ultrafast Dynamics of Lasing Semiconductor Nanowires". *Nano Letters* **2015**, *15 (7)*, 4637-4643.
11. Mayer, B. *et al.* "Long-term mutual phase locking of picosecond pulse pairs generated by a semiconductor nanowire laser". *Nature Communications* **2017**, 15521.
12. Stettner, T. *et al.* "Coaxial GaAs-AlGaAs core-multishell nanowire lasers with epitaxial gain control". *Applied Physics Letters* **2016**, *108*, 011108.
13. Wirths, S. *et al.* "Room-Temperature Lasing from Monolithically Integrated GaAs Microdisks on Silicon". *ACS Nano* **2018**, 12 (3).
14. Baumgartner, Y. *et al.* "Monolithic integration of InAlAs/InGaAs quantum-well on InP-OI micro-substrates on Si for infrared light sources". *IEEE 14th International Conference on Group IV Photonics (GFP)* **2017**, 173.
15. Shchekin, O.B. *et al.* "High temperature performance of self-organised quantum dot laser with stacked p-doped active region". *Electronics Letters.* **2002,** *38*, 14.


1041-1135 (c) 2019 IEEE. Personal use is permitted, but republication/redistribution requires IEEE permission. See http://www.ieee.org/publications_standards/publications/rights/index.html for more information.